OXFORD

Human Molecular Genetics, 2017, Vol. 26, No. 13 2398–2411

doi: 10.1093/hmg/ddx128
Advance Access Publication Date: 7 April 2017
Original Article

ORIGINAL ARTICLE

Fat mass and obesity-associated (FTO) protein regulates adult neurogenesis

Liping Li[1,2,3,†], Liqun Zang[1,2,3,†], Feiran Zhang[4,†], Junchen Chen[2,3], Hui Shen[2,3], Liqi Shu[4,5], Feng Liang[2,3], Chunyue Feng[2], Deng Chen[6], Huikang Tao[2], Tianlei Xu[7], Ziyi Li[7], Yunhee Kang[4], Hao Wu[7], Lichun Tang[8], Pumin Zhang[8], Peng Jin[4,*], Qiang Shu[2,*] and Xuekun Li[2,3,*]

[1]Institute of Genetics, College of Life Sciences, Zhejiang University, Hangzhou 310058, China, [2]The Children's Hospital, School of Medicine, Zhejiang University, Hangzhou 310052, China, [3]The Institute of Translational Medicine, School of Medicine, Zhejiang University, Hangzhou 310029, China, [4]Department of Human Genetics, Emory University School of Medicine, Atlanta, GA 30322, USA, [5]School of Medicine and Health Sciences, George Washington University, Washington, DC 20037, USA, [6]State Key Laboratory of Medical Molecular Biology, Department of Biochemistry and Molecular Biology, Institute of Basic Medical Sciences, Chinese Academy of Medical Sciences and School of Basic Medicine, Peking Union Medical College, Beijing 100005, China, [7]Department of Biostatistics and Bioinformatics, Rollins School of Public Health, Emory University, Atlanta, GA 30322, USA and [8]National Center for Protein Sciences Beijing, Life Sciences Park, Beijing 102206, China

*To whom correspondence to be addressed. Tel: 404-727-3729; Fax: 404-727-3949; Email: peng.jin@emory.edu (P.J.); Tel: 86-571-86670006; Fax: 86-571-86658672; Email: shuqing@zju.edu.cn (Q.S.); Tel: 86-671-86971653; Fax: 86-571-86658672; Email: xuekun_li@zju.edu.cn (X.L.)

Abstract

Fat mass and obesity-associated gene (*FTO*) is a member of the Fe (II)- and oxoglutarate-dependent AlkB dioxygenase family and is linked to both obesity and intellectual disability. The role of FTO in neurodevelopment and neurogenesis, however, remains largely unknown. Here we show that FTO is expressed in adult neural stem cells and neurons and displays dynamic expression during postnatal neurodevelopment. The loss of FTO leads to decreased brain size and body weight. We find that FTO deficiency could reduce the proliferation and neuronal differentiation of adult neural stem cells *in vivo*, which leads to impaired learning and memory. Given the role of FTO as a demethylase of N6-methyladenosine (m^6A), we went on to perform genome-wide m^6A profiling and observed dynamic m^6A modification during postnatal neurodevelopment. The loss of FTO led to the altered expression of several key components of the brain derived neurotrophic factor pathway that were marked by m^6A. These results together suggest FTO plays important roles in neurogenesis, as well as in learning and memory.

Introduction

In adult vertebrate brain, neurogenesis driven by adult neural stem cells (aNSCs) produces new neurons in limited regions, such as the subventricular zone (SVZ) of the lateral ventricles and the subgranular zone (SGZ) of the dentate gyrus of the hippocampus (1). The newborn neurons integrate into neuronal circuits and perform physiological functions. Dysfunction of adult neurogenesis can lead to impaired learning and memory and

[†]These authors contributed equally to this work.

Received: January 24, 2017. **Revised:** March 12, 2017. **Accepted:** March 28, 2017

contribute to the pathogenesis of depression, epilepsy and neurodegenerative diseases (2,3). Earlier studies have shown that adult neurogenesis is regulated by many factors, including genetics, signaling pathways, growth factors and metabolic state, as well as epigenetic factors (1,4–8).

Fat mass and obesity-associated gene (*FTO*) is linked to human obesity (9,10). Previous studies revealed FTO plays pivotal roles in adipogenesis and energy homeostasis (11). *FTO*-deficient mice display postnatal growth retardation and reduced food intake, with a significant reduction of adipose tissue (10,12), whereas the overexpression of FTO caused obesity in mice (9). FTO protein is also found to be highly abundant in brain and is associated with reduced brain volume in adolescents and older people (12–14). *FTO* gene deficiency enhances the retention of fear memory (15) and also impairs dopamine receptor 2- and 3-dependent control of neuronal activity and locomotor behavioral responses (16). These studies indicate that FTO plays important roles in normal brain function.

Molecularly, FTO was identified as an RNA demethylase, and its expression level inversely correlates with N6-methyladenosine (m^6A) level (17). m^6A is a conserved internal modification found in almost all eukaryotic nuclear RNAs, as well as in some viral RNA, such as Rous sarcoma virus, which replicates inside host nuclei (18,19). The discoveries of functionally important methylases and demethylases, including FTO, together with the recently revealed m^6A distributions in mammalian transcriptomes, are strong indicators of regulatory functions for this dynamic modification (20,21). m^6A is developmentally regulated and increases during postnatal brain development (22). The role of m^6A in neurogenesis remains to be defined; however, the expression of genes involved in m^6A methylation and demethylation could be differentially regulated during neuronal differentiation, suggesting a potential role for this RNA modification in neuronal development (Kang and Jin, unpublished data). As a demethylase of m^6A, the role of FTO in the regulation of adult neurogenesis remains largely unknown.

Here we show that FTO is expressed in aNSCs and neurons and displays dynamic expression during postnatal neurodevelopment. The loss of FTO leads to decreased brain size and body weight. We found that FTO deficiency could reduce the proliferation and neuronal differentiation of aNSCs *in vivo*, which leads to impaired learning and memory. We further performed genome-wide m^6A profiling and observed dynamic m^6A modification during postnatal neurodevelopment. Interestingly, the loss of FTO led to the altered expression of several key components of the brain derived neurotrophic factor (BDNF) pathway that were marked by m^6A. These results together suggest FTO plays important roles in neurogenesis, learning and memory.

Results

Dynamic expression of FTO during postnatal neurodevelopment

To determine whether FTO plays any role in adult neurogenesis, we first examined the expression of FTO in mouse brain using immunofluorescence staining. FTO protein was detected in Nestin$^+$ aNSCs (Fig. 1A). Consistent with previous studies (13,16), we also found that FTO is highly expressed in NeuN$^+$ mature neurons (Fig. 1B). During postnatal development [from postnatal day 1 (P1) to postnatal 8 weeks (P8W)], western blot results showed that the expression of FTO increased from postnatal day 1 (P1) to postnatal 2 weeks (P2W) and adulthood (postnatal 8 weeks, P8W) (Fig. 1C and D).

We next examined the *FTO* knockout (KO) mice generated previously (12) (Supplementary Material, Fig. S1A). In the brains of KO mice, *Fto* transcripts were not detected (Supplementary Material, Fig. S1B). We found that the constitutive loss of *Fto* led to lower body weight in postnatal 3- (weaning time) and 8-week-old female and male mice, respectively (Supplementary Material, Fig. S1C–F). Furthermore, the loss of *FTO* could result in a smaller brain, and distinct brain structures were also smaller compared to WT mice (Fig. 1E–G and Supplementary Material, Fig. S1G). Together, these results suggest that FTO plays important roles in neurodevelopment.

The loss of FTO leads to reduced proliferation of aNSCs *in vivo*

To determine the role of FTO in adult neurogenesis, we injected adult mice with BrdU as illustrated in Figure 2A (50 mg/kg, 6 injections with an interval of 4 h, i.p.). Twenty-four hours after the last BrdU injection, mice were scarified for analyses. BrdU-positive (BrdU$^+$) cells were detected in the hippocampus of both WT and KO mice, indicating the proliferation capacity of aNSCs (Fig. 2B–G). The majority of BrdU$^+$ cells were localized in the subgranular zones (SGZ) of the hippocampus of both WT and KO mice, suggesting the aNSCs resided mainly in the SGZ and had not initiated migration yet. Quantification results indicated that the numbers of BrdU$^+$ cells were significantly decreased in KO mice compared to WT mice (Fig. 2H).

We further analyzed the effect of the loss of Fto on the proliferation of aNSCs in the subventricular zone (SVZ) of the lateral ventricles. Similar to the SGZ region, BrdU positive (BrdU$^+$) cells could be also detected in the SVZ region of both WT and KO mice (Fig. 2I–J). Quantification results indicated that the numbers of BrdU$^+$ cells were also significantly decreased in KO mice compared to WT mice (Fig. 2K). Furthermore, the numbers of BrdU$^+$ cells were significantly higher in SVZ regions than in SGZ regions of both WT and KO mice. Together, these results indicate that the loss of *FTO* significantly reduced the numbers of aNSCs in both the SGZ and SVZ regions.

The loss of *FTO* decreases the neuronal differentiation of aNSCs

To determine the role of FTO in the neuronal differentiation of aNSCs, adult WT and KO mice were injected with BrdU as illustrated in Figure 3A (50 mg/kg, i.p., 2 times/day for 3 days). The mice were sacrificed 1 week after the final BrdU injection. BrdU-Ki67 double immunofluorescence staining revealed the existence of aNSCs in the SGZ regions of the hippocampus in both WT and KO mice (Fig. 3B–I). Quantification results showed that the numbers of BrdU$^+$ cells were significantly decreased in KO mice compared to WT mice (Fig. 3R). Since the decreased proliferation could be due to the lengthened cell cycle of NSCs or fewer numbers of NSCs, we next performed immunofluorescence staining of Ki67, a cell cycle marker. Quantification results showed that the numbers of Ki67$^+$ cells were decreased in KO mice (Fig. 3S). These results suggest the loss of *Fto* could reduce the pool of aNSCs in the SGZ region.

Next we carried out BrdU-DCX double immunofluorescence staining to study early neuronal differentiation in WT and KO mice (Fig. 3J and Q). The numbers of total DCX$^+$ and BrdU$^+$DCX$^+$ cells were significantly decreased in KO mice (Fig. 3T and U). Furthermore, the percentage of BrdU$^+$DCX$^+$ in total BrdU$^+$ cells was also decreased in KO mice (Fig. 3V). We found that the

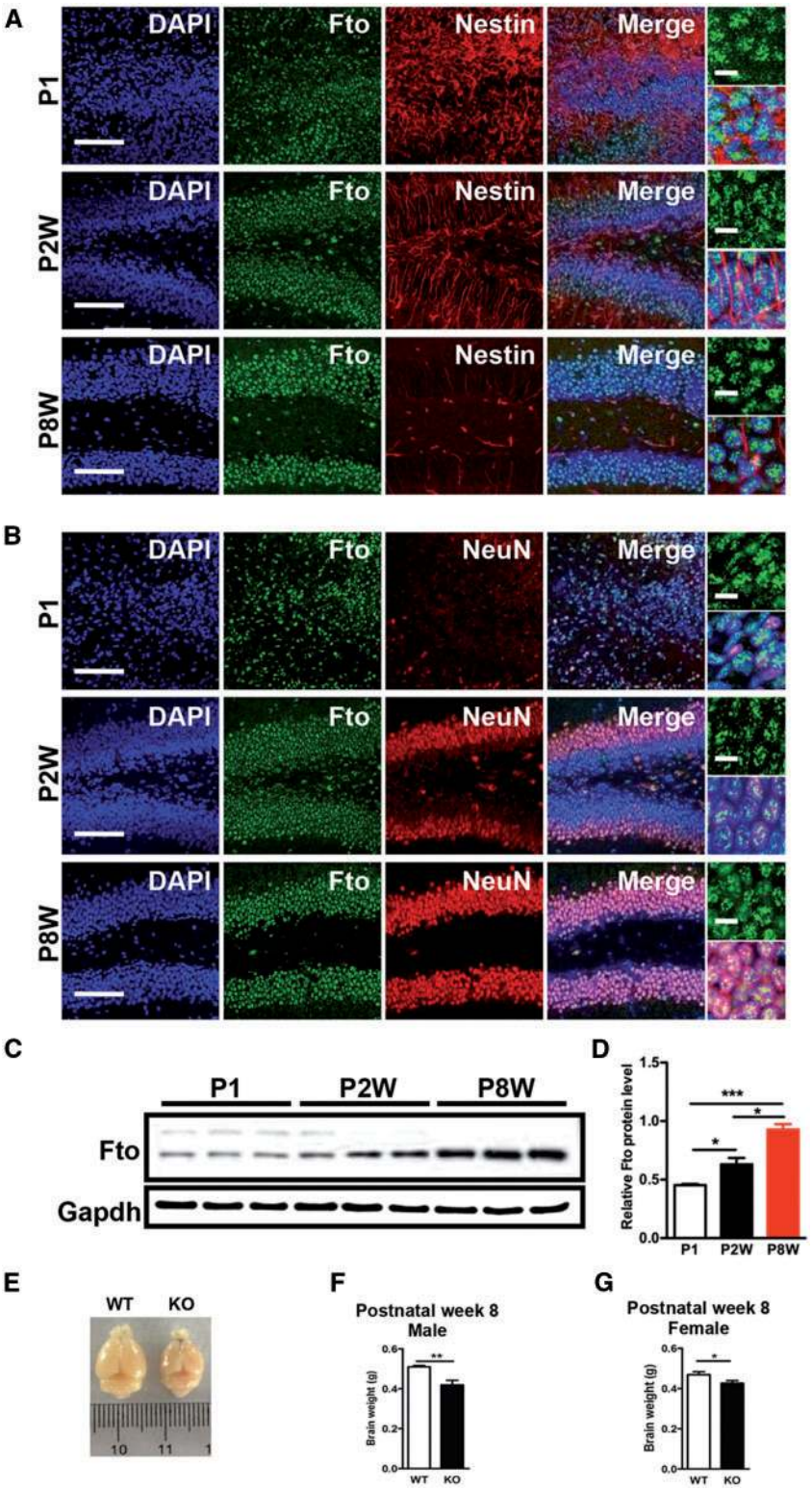

Figure 1. Dynamic expression of FTO during postnatal brain development. (**A**) Immunofluorescence staining shows the expression of FTO in Nestin$^+$ adult neural stem cells (aNSCs). (**B**) Immunofluorescence staining shows the expression of FTO in NeuN$^+$ mature neurons. During postnatal brain development [from postnatal day 1 (P1), postnatal 2-week (P2W), and postnatal 8-week (P8W, adult)], Nestin$^+$ cells gradually decrease, while NeuN$^+$ cells and the expression of FTO increase in the hippocampus. (**C**, **D**) Western blot analysis (C) and quantitative results (D) revealed that the FTO protein level increases during postnatal brain development ($n = 3$). GAPDH was used as a loading control. Data are presented as mean ± S.E.M., unpaired *t*-test, $^*P < 0.05$; $^{**}P < 0.01$. (**E**) Representative images show *FTO* knockout (KO) led to a smaller brain size compared to wild-type (WT) mice. (**F**, **G**) The brain weights of both female and male *FTO* KO mice are less than age- and gender-matched WT mice. N = 14 WT/16 KO (male); $n = 12$ WT/13 KO (female). Data are presented as mean ± S.E.M., unpaired *t*-test, $^*P < 0.05$; $^{**}P < 0.01$; $^{***}P < 0.001$. Scale bar: 100 μm in A and B and 10 μm in the far right panels.

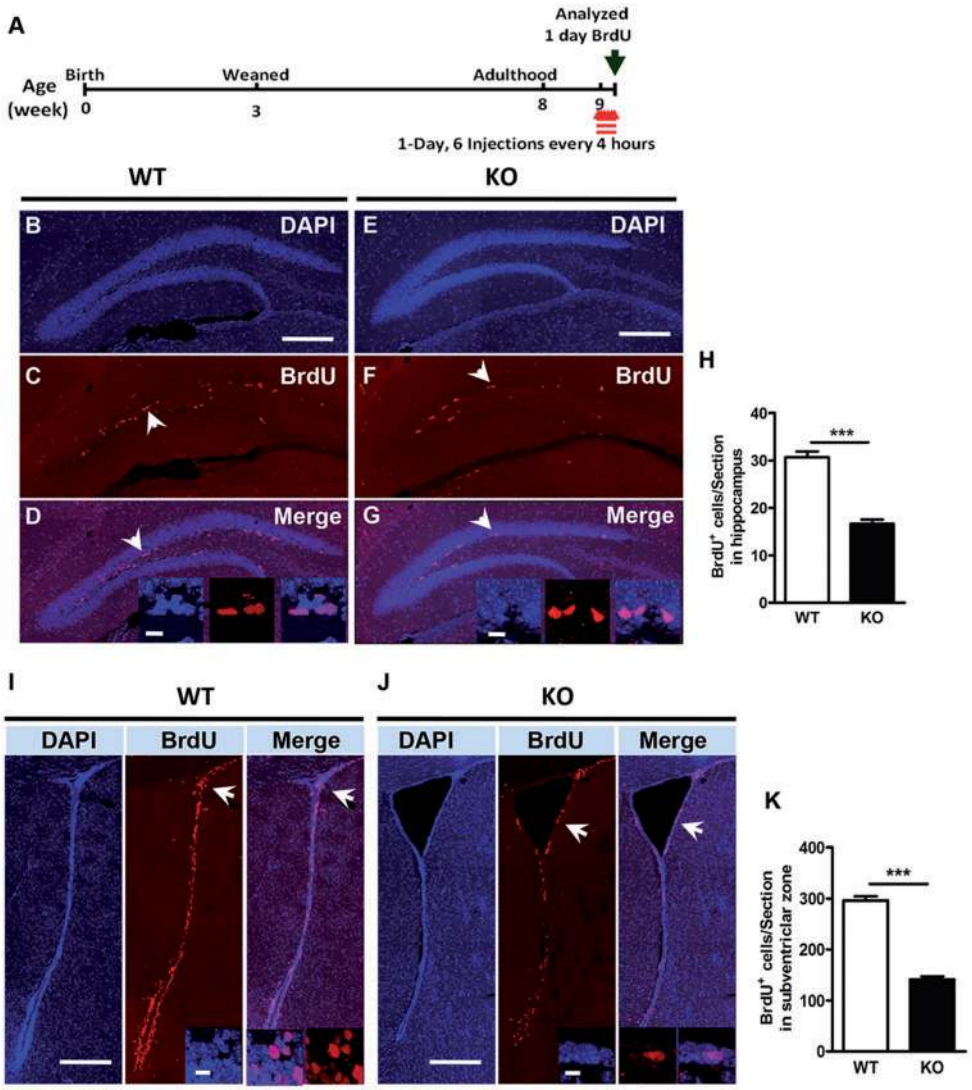

Figure 2. The loss of FTO reduces the proliferation of aNSCs in hippocampus and lateral ventricles. (**A**) Schematic illustration of the proliferation assay of aNSCs. Adult WT and KO mice were injected with BrdU (six doses, 50 mg/kg, i.p.) every 4 h within a 24-h period. (**B–G**) Representative images showing the BrdU$^+$ aNSCs localized in the subgranular zone of the dentate gyrus (DG) of the hippocampus in WT and *FTO* KO mice. Scale bars: 200 μm (B–G) and 10 μm in highly magnified inserts. (**H**) Quantification results show the total numbers of BrdU$^+$ cells significantly decreased in FTO KO mice compared to WT mice. (**I–J**) Representative images showing the BrdU$^+$ cells in the subventricular zone (SVZ) of WT and FTO KO mice. Scale bars: 200 μm in I–J and 10 μm in highly magnified inserts. (**K**) Quantitative analysis indicated fewer BrdU$^+$ cells in the SVZ of FTO KO mice compared with WT mice. WT, $n = 5$; KO, $n = 6$. Unpaired *t*-test, $^*P < 0.05$, $^{***}P < 0.001$.

length of dendrites was also significantly reduced in KO mice (Fig. 3W and Supplementary Material, Fig. S2A–H). The loss of *FTO* did not alter the soma positioning of aNSCs in the SGZ region when analyzed 1 week post-BrdU injection (Supplementary Material, Fig. S2L–O). However, FTO deficiency significantly reduced the number of cells positioned in the SGZ and increased the number of cells positioned at the molecular cell layer when analyzed 4 weeks post-BrdU injection (Supplementary Material, Fig. S2P and Q). In the SVZ region, we also saw a significant decrease of BrdU single- and BrdU-DCX double-positive (BrdU$^+$DCX$^+$) cells (Supplementary Material, Fig. S3A–J). Together, these results suggest that the loss of FTO could reduce immature neuronal differentiation of aNSCs.

To study the mature neuronal differentiation of aNSCs, BrdU-NeuN double immunostaining was performed 4 weeks after the final BrdU administration. Immunostaining revealed that the majority of BrdU$^+$ cells migrated away from the SGZ regions compared to the 1-day time point (Fig. 4A–H). Newborn neurons, BrdU$^+$NeuN$^+$ cells could be found in both WT and KO cells (Fig. 4I–P). Quantification results suggest that the numbers of BrdU$^+$ and BrdU$^+$NeuN$^+$ cells were significantly decreased in KO mice (Fig. 4Q and R). Furthermore, the percentage of newborn neurons, indicated by BrdU$^+$NeuN$^+$ in total BrdU$^+$ cells, was also decreased in KO mice (Fig. 4S). There was no significant difference for the survival rate of aNSCs between WT and *FTO* KO mice (Fig. 4T). Consistently, we saw no significant change in the number of apoptotic cells in WT and KO mice using a TUNEL assay, suggesting the loss of *FTO* did not alter apoptosis (Supplementary Material, Fig. S4). Together, these results suggest the loss of *FTO* could lead to reduced mature neuronal differentiation.

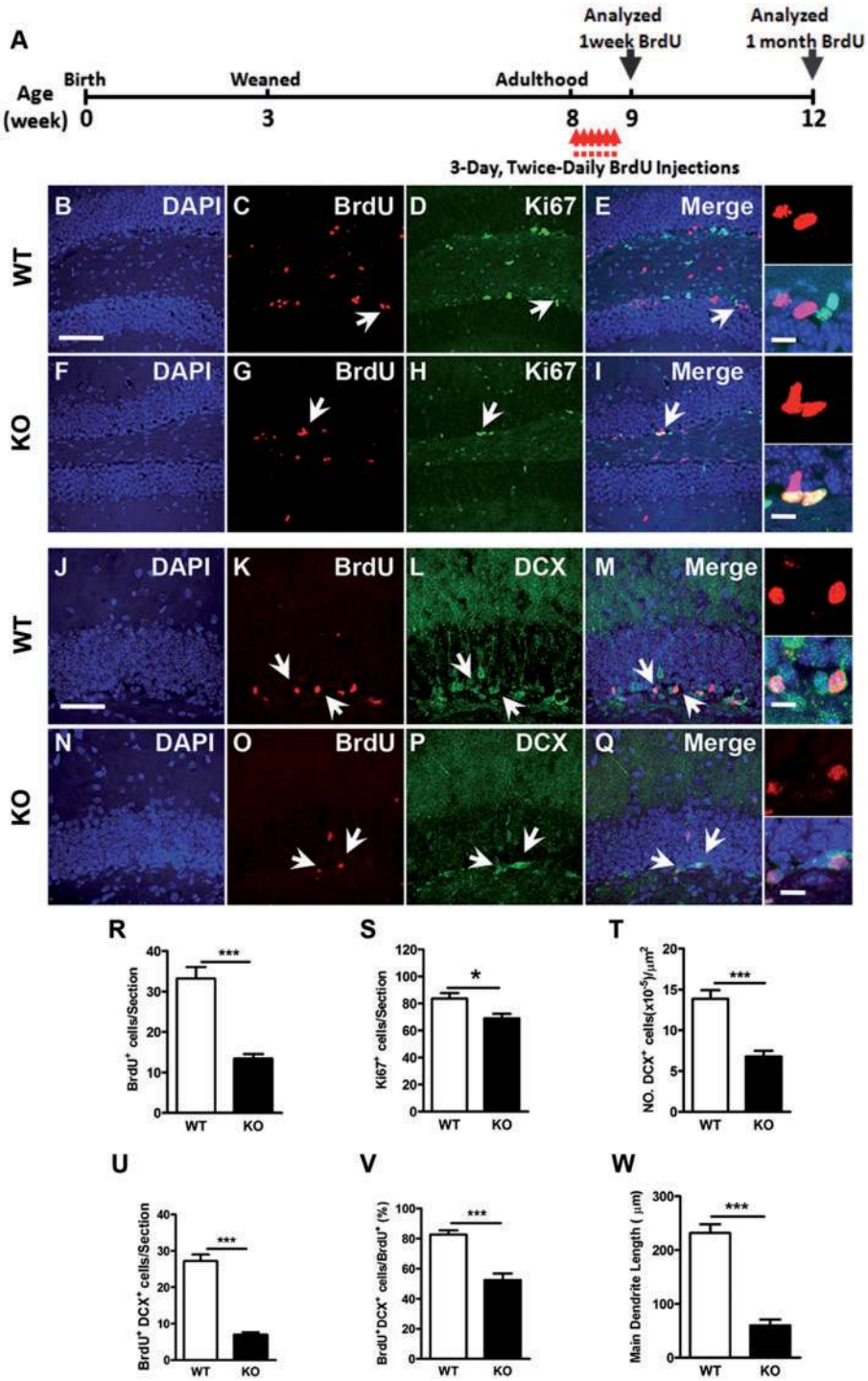

Figure 3. FTO deficiency impairs the immature and mature neuronal differentiation of aNSCs. (**A**) Schematic illustration of the differentiation assay of aNSCs. WT and KO male mice received BrdU injections (50 mg/kg, i.p., twice daily with an 8-h interval for three consecutive days) at the age of 8 weeks old. One and four week(s) after the final BrdU injection, mice were sacrificed for the analysis of immature and mature neuronal differentiation of aNSCs, respectively. (**B–I**) Representative immunofluorescence staining images showed $BrdU^+$ and $Ki67^+$ aNSCs in the hippocampus of WT and KO mice. Scale bar: 80 μm in B–I and 10 μm in highly magnified panels. (**J, Q**) Representative immunofluorescence staining images show $BrdU^+$ aNSCs differentiated into immature DCX^+ neurons in WT and KO mice. Scale bar: 50 μm in J–Q and 10 μm in highly magnified panels. (**R, S**) Quantitative analysis indicated a significant decrease of $BrdU^+$ cells (R) and $Ki67^+$ cells (S) in the DG of KO mice compared to WT mice. (**T**) Quantification results demonstrate that KO mice had fewer DCX^+ immature neurons per volume in DG. (**U, V**) The number and the percentage of newborn neurons ($BrdU^+$ DCX^+) were significantly decreased in KO mice compared to WT mice. (**W**) The main dendrite length of DCX^+ cells in KO was significantly shorter compared to WT. WT, $n = 8$; KO, $n = 9$. Unpaired *t*-test, $^*P < 0.05$; $^{**}P < 0.01$; $^{***}P < 0.001$.

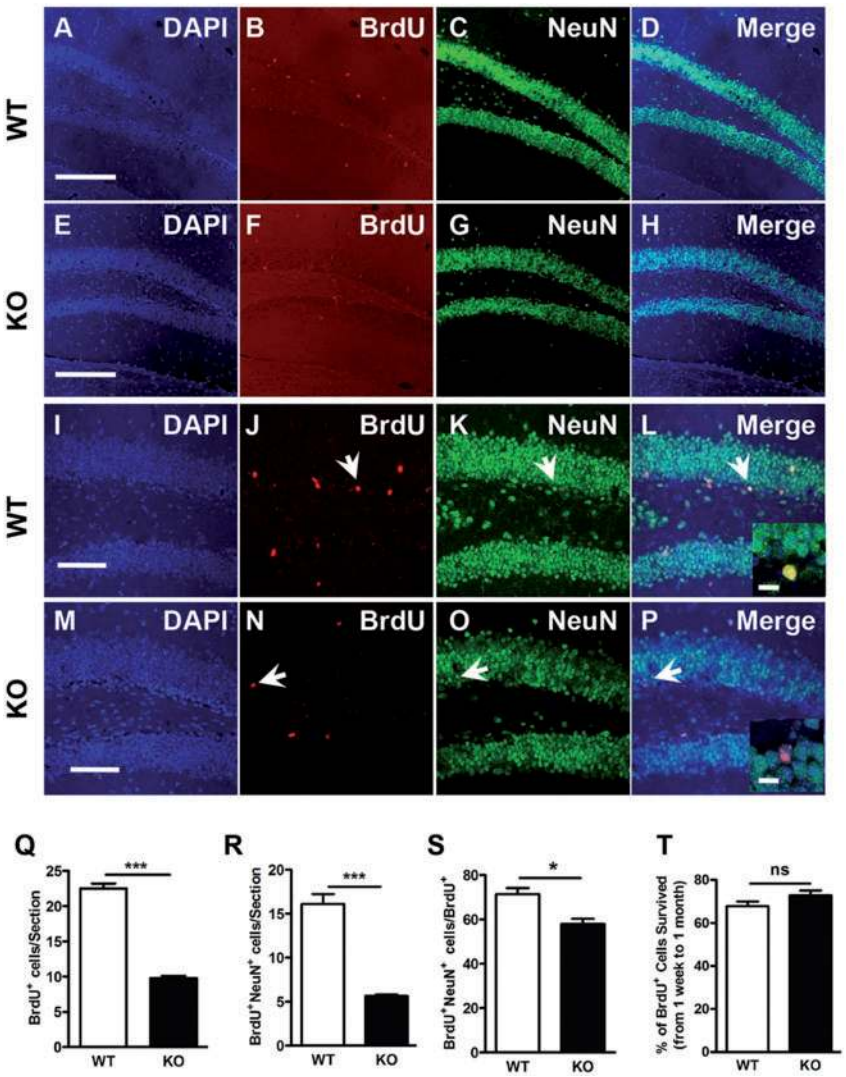

Figure 4. The loss of FTO leads to a decrease of newborn neurons in adult mice. (**A–H**) Representative images showing fewer BrdU$^+$ cells localized in the hippocampus of KO mice compared to WT mice one month after the final BrdU injection. Scale bar: 200 μm. (**I–P**) Representative images showing fewer newly born mature neurons (BrdU$^+$NeuN$^+$) in KO mice compared to WT mice. Scale bar: 80 μm in I–P and 10 μm in highly magnified inserts. (**Q**) Quantification of BrdU$^+$ cells per section showing that FTO deletion led to decreased neuronal differentiation in DG. (**R**) Quantitative analysis of BrdU$^+$NeuN$^+$ cells per section revealed that the newborn cells in KO mice obstructively differentiated into NeuN$^+$ neurons. (**S**) Meanwhile, newborn cells of KO mice showed a lower percentage of mature neurons. (**T**) However, there was no difference in surviving newborn cells in the DG. WT, $n = 15$; KO, $n = 13$. Unpaired *t*-test, $^*P < 0.05$; $^{**}P < 0.01$; $^{***}P < 0.001$; ns: no significant difference.

The loss of *FTO* impairs learning and memory

Since adult neurogenesis has been linked to learning and memory, we next explored whether the impaired neurogenesis caused by the loss of *Fto* could alter learning and memory. We first performed the Morris water maze and eight-arm maze tests. Figure 5A shows representative images of the swimming routes of WT and KO mice. WT and KO mice did not show a significant difference in swimming velocity throughout the 4-day training trials (Fig. 5B). From day 1 to day 3, WT and KO mice displayed a similar swimming path and escape latency (Fig. 5C and D). On the fourth day, KO mice exhibited impaired learning capacity compared to WT mice (Fig. 5C and D). Short-term memory was tested 24 h after the 4-day training period. The *Fto* KO mice displayed longer escape latency, fewer times crossing the platform, increased time to first reach the platform, and reduced time in the target quadrant (Fig. 5E–H), suggesting a deficiency in short-term memory.

We further tested spatial learning and memory with the eight-arm radial maze (Fig. 5I). During the first 2 days of training, WT and KO mice displayed similar learning capacities. From the third day to the end of the test (the seventh day), *FTO* KO mice exhibited a higher reference error ratio compared to WT mice (Fig. 5J and K). Meanwhile, the total entries to the arms of *FTO* KO mice were significantly higher than WT mice (Fig. 5L). Together, these results suggest that *FTO* deficiency impaired the learning and memory of mice.

The loss of *Fto* results in the increase of global m6A and dysregulated gene expression in hippocampus

Considering the demethylase activity of FTO, we speculated that FTO could regulate adult neurogenesis by modulating RNA methylation. We then carried out the m^{6}A dot-blot with hippocampal RNA of adult WT and *FTO* KO mice (Supplementary Material, Fig. S5A). The dot-blot results showed that the level of

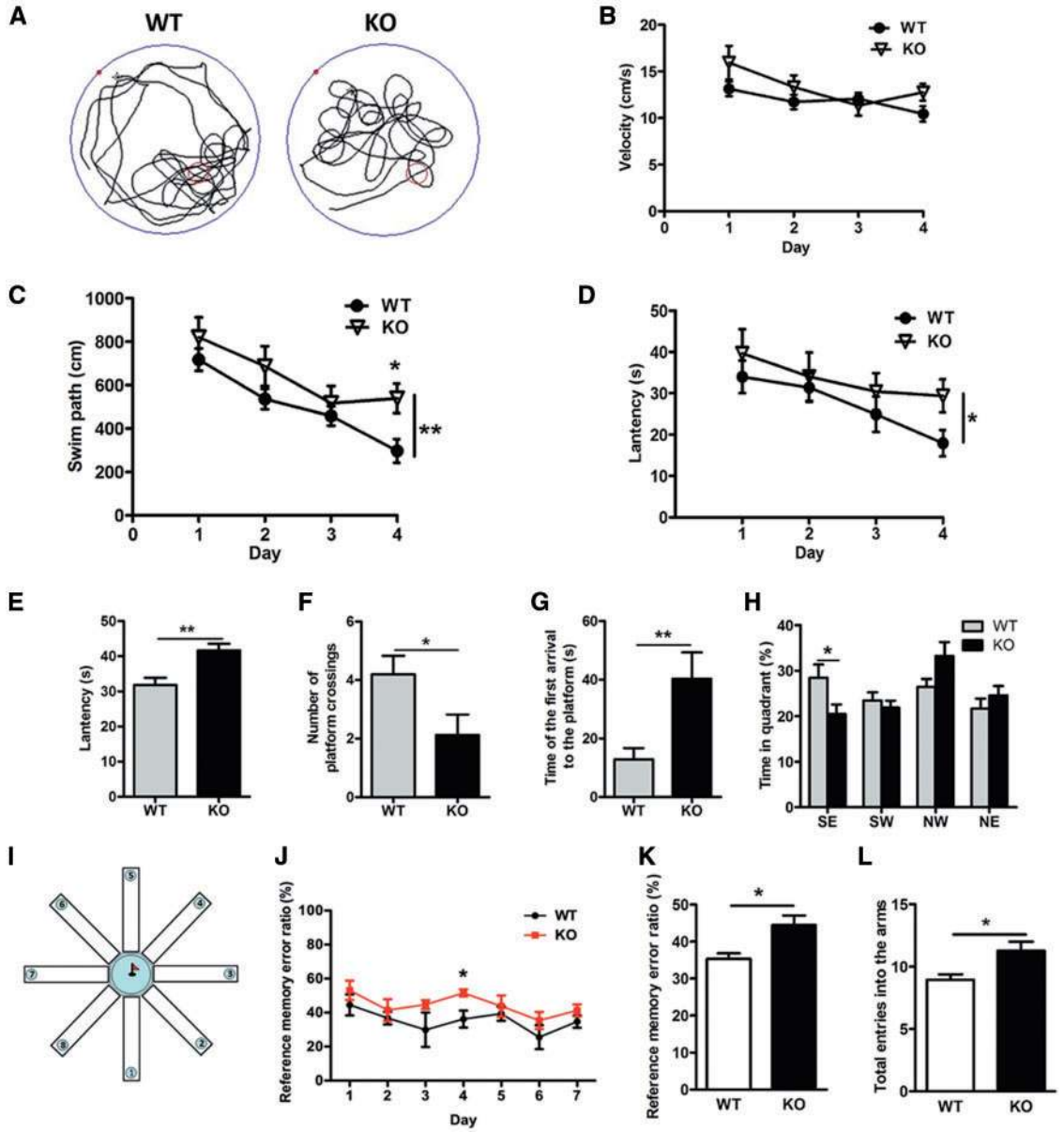

Figure 5. FTO depletion impairs spatial learning and memory of mice. (**A**) Representative images showing the swim path of the MWM test of WT and KO mice. (**B–D**) The swim velocity (B), swim path (C) and escape latency (D) of WT and KO mice during 4 days' navigation training. (**E**) Escape latency of WT and KO mice in the short-term trial. (**F**) The number of platform crossings in the short-term trial. (**G**) Time to arrive at the platform for the first time in the probe trial. (**H**) The percentage of time in the target quadrant and other quadrants. (**I**) Schematic illustration of the eight-arm maze test. (**J**) The ratio of reference memory error for each day during 7 days of testing. (**K**) The mean of the ratio of reference memory error during 7 days of testing. (**L**) Total entries into the arms. WT, $n = 10$; KO, $n = 8$. Unpaired *t*-test, $^{*}P < 0.05$; $^{**}P < 0.01$; $^{***}P < 0.001$.

m6A was significantly increased in *FTO* KO mice compared to WT mice (Supplementary Material, Fig. S5B). Further, we performed m^{6}A RIP-seq using RNA from the hippocampus of both young (2-week-old) and adult (6-week-old) WT mice. In total, 23,480 and 16,212 m^{6}A peaks were identified in young and adult mice, respectively (Supplementary Material, Table S1). These peaks were associated with 8,049 and 6,388 genes in young and adult mice, respectively: 2,414 unique genes in young mice, 753 unique genes in adult mice and 5,635 genes overlapping between young and adult mice (Fig. 6A, Supplementary Material, Table S2). m^{6}A peak analysis showed that the distribution of m^{6}A peaks across the length of mRNA transcripts was similar between WT young and adult mice (Supplementary Material, Fig. S6A). More m^{6}A peaks located in the first exon of hippocampal transcripts in young mice compared to adult mice (Supplementary Material, Fig. S6B). The density of m^{6}A peaks increased more sharply when entering the last exon than when approaching the stop codon in both young and adult mice (Supplementary Material, Fig. S6B). It was also found that the majority of m^{6}A peaks containing transcripts only had one m^{6}A peak (Fig. 6C). To exclude the possibility that m^{6}A peak distribution was caused by immunoprecipitation (IP), we then analyzed the fold enrichment of high-confidence m^{6}A peaks that were present in both biological replicates. IP ratio was calculated as normalized read density within a peak in IP samples divided by normalized read density within the corresponding regions in

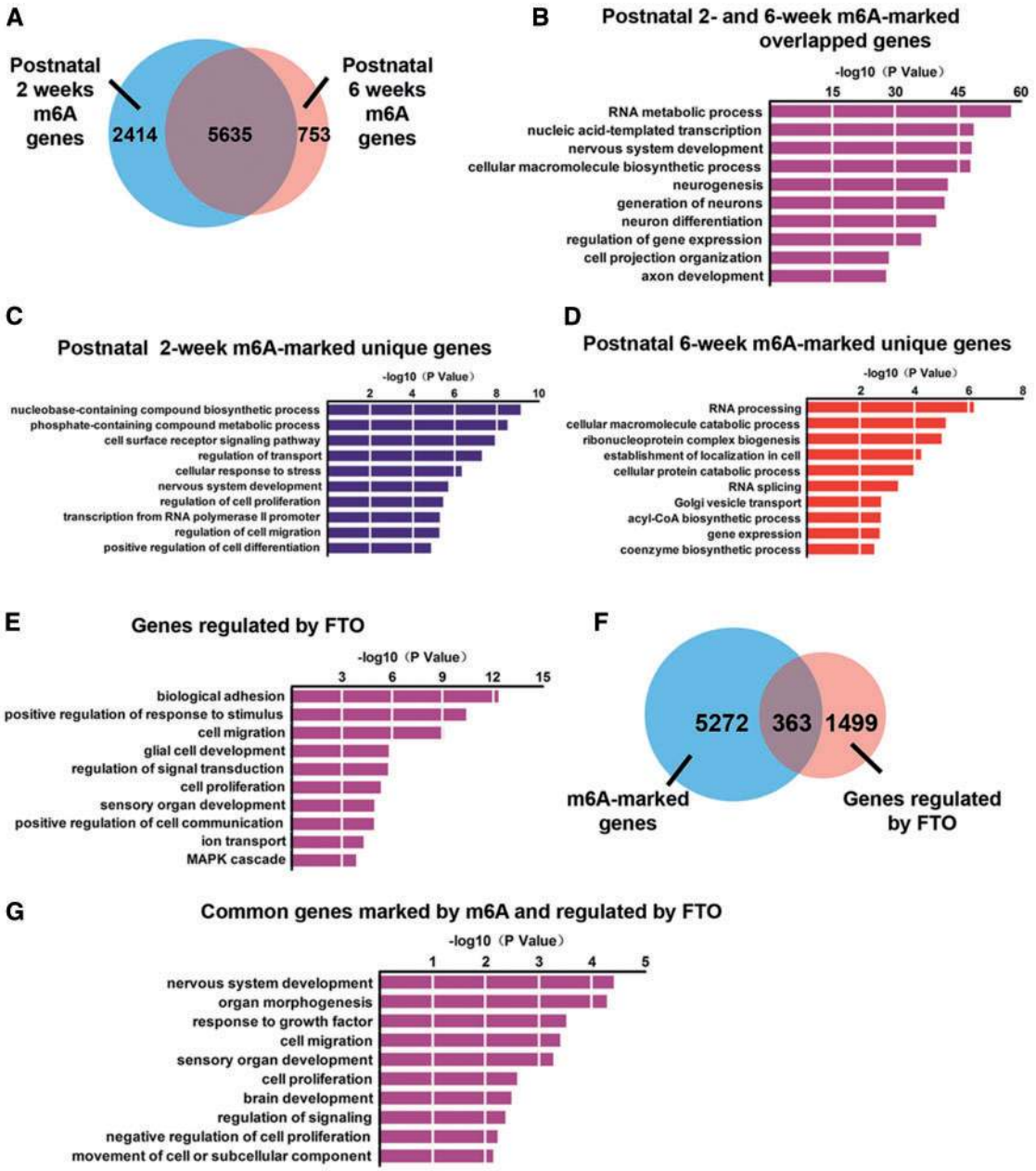

Figure 6. m^{6}A-RIP-seq reveals dynamic m^{6}A modification and its correlation with altered gene expression caused by the loss of FTO. (**A**) Venn diagram illustrating the numbers of m6A-modified unique and common mRNA transcripts in the hippocampus of young (postnatal 2 weeks) and adult (postnatal 6 weeks) WT mice, respectively. (**B**) Gene ontology analysis results of the m^{6}A-modified common genes shared between young and adult mice. (**C, D**) Gene ontology analysis results of the m^{6}A-modified unique genes identified in young (C) and adult (D) mice, respectively. (**E**) Gene ontology analysis results of the altered genes in the hippocampus of *FTO* KO mice. (**F**) Venn diagram illustrating the m^{6}A-modified common genes identified in young and adult mice and genes with altered expression identified in adult *FTO* KO mice. (**G**) Gene ontology analysis results of the overlapping genes between m^{6}A-modified genes and altered genes in KO mice.

input samples. We found that the distribution of IP ration was similar between young and adult mice, and more than 80% m^{6}A peaks showed at least 5-fold enrichment, suggesting a *bona fide* identity of identified m^{6}A peaks (Supplementary Material, Fig. S6D, GEO: GSE94098).

Gene ontology (GO) analysis showed 5,635 overlapping genes (termed as m^{6}A modified common genes) were highly enriched in pathways related to RNA metabolism, regulation of transcription, neurogenesis and neuronal development, among others (Fig. 6B). Further, 2,414 unique genes identified in young mice were significantly enriched in pathways related to RNA metabolism, development, cell proliferation, and differentiation, among others (Fig. 6C), while those 753 unique genes identified in adult mice were enriched in pathways related to mRNA processes, cell division, and transport, among others (Fig. 6D).

To determine the effect of FTO on gene expression, we carried out RNA-seq using RNA isolated from the hippocampus of adult WT and *FTO* KO mice. We found altered expression of 1,862 genes (termed as Fto modulated genes): 494 genes were upregulated and 1,368 genes downregulated (Supplementary Material, Table S3, Fig. 6E). Further analyses revealed that 363 genes overlapped between m^{6}A modified common genes and

Fto-modulated genes (Fig. 6F), which were highly enriched in pathways related to neuronal development, cell proliferation, and migration, among others (Fig. 6G, Supplementary Material, Table S4). The analysis of a previously published data (16) also showed in total 1518 specific m^6A modification marked genes, 164 genes showed altered expression (Supplementary Material, Fig. S5C and D).

Previous studies have shown that BDNF plays important roles in neuronal development, and FTO regulates the expression of BDNF (23–27). Among m^6A modification marked transcripts, we found that transcripts of several components of BDNF signaling pathway were marked with m^6A at both 2 and 6 week (Supplementary Material, Fig. S7A). Consistently, the reanalysis of previous published data also revealed that these transcripts were marked with m^6A modification in the midbrain of WT and *FTO* KO mice (16) (Supplementary Material, Fig. S7B). Hippocampal RNA-seq data also showed that the expression of several genes of the nerve growth factor receptor (NGFR)-BDNF pathway was altered.

Next, we performed western blot analysis and found that BDNF levels were significantly decreased in the hippocampus tissues of KO mice (Fig. 7A and B). Akt is a downstream target of BDNF, and phosphorylated Akt levels (p-Akt, Ser473 and Thr308) were decreased in KO mice, while the level of total Akt was not altered (Fig. 7A, C–E). While the total level of p70S6K1, another component of the BDNF signaling pathway, did not change, the level of phosphorylated p70S6K1 (p-p70S6K1, Thr389) was deceased in KO mice (Fig, 7F, G). QRT-PCR results showed that the mRNA levels of BDNF, PI3K, Akt2, Akt3 and mTOR were also decreased (Fig. 7H). Considering the decrease of neurogenesis in the mouse brain from 2-week to 6-week, we further analyzed m^6A modification in a few neurogenesis related transcripts, including Nestin, Sox2 and NeuroD. We observed that m^6A marked these transcripts both at 2- and 6-week time point (Supplementary Material, Fig. S7). Interestingly, m^6A modification on these transcripts decreases from 2-week to 6-week (Supplementary Material, Fig. S8). These results together suggest the loss of FTO could alter the BDNF signaling pathway and the alteration of FTO-catalyzed m^6A modification could contribute to impaired adult neurogenesis through modulating BDNF pathway (Fig. 7I).

Discussion

FTO is linked to human obesity (9,10), and previous work revealed that *FTO* plays pivotal roles in adipogenesis and energy homeostasis (11). *FTO*-deficient mice display postnatal growth retardation, reduced food intake and a significant reduction in adipose tissue (10,12), while overexpression of *FTO* can cause obesity in mice (9). In brain, FTO is widely expressed and highly enriched in neurons (12,14). *FTO* variants are associated with reduced brain volume and affect the activity of brain regions important for emotion and neural response to food images (14,28–30). The modulation of FTO can also impact the CREB signaling pathway and alter the neuronal responses to fear and cocaine (15,16,23). These studies strongly suggest that FTO could play important roles in modulating brain function. Our work presented here demonstrates a role for FTO in the regulation of adult neurogenesis. Loss of *Fto* leads to a smaller sized whole brain and distinct brain regions in mice. Furthermore, the loss of *FTO* not only reduces the proliferation of aNSCs but also inhibits neuronal differentiation in both the SVZ and SGZ regions of adult mice. FTO-deficient mice display impaired spatial learning and memory. We observed dynamic m^6A modification during postnatal neuronal development. m^6A modification distributes across the exons of transcripts with a dramatic enrichment on the last exon. m^6A modification also marks some neurogenesis-related transcripts, including BDNF. The expression of a subset of genes, including *BDNF*, is dysregulated in the absence of FTO, and the altered BDNF signaling could contribute to the impaired adult neurogenesis associated with the loss of *Fto*.

Epigenetic modifications are known to play important roles in regulating the lineage commitment, specification, and self-renewal of neural stem cells during adult neurogenesis (4–8,31,32). In eukaryotes, m^6A RNA methylation is deposited by methyltransferase-like 3 (Mettl3) and 14 (Mettl14) and is removed by demethylase FTO and ALKBH5, which are abundant and conserved across different species (33,34). Although an earlier study showed conflicting results (35), recent works have found that Mettl3-depleted embryonic stem cells failed to undergo differentiation and lock in the pluripotency state (36,37). FTO is found to be highly expressed in neuronal cells (12,13) and can regulate neuronal function in mice (15,38,39). Our study reveals that FTO is highly expressed in aNSCs, as well. The loss of FTO leads to fewer $Ki67^+$ and $BrdU^+$ cells, suggesting a diminished pool of aNSCs and a decreased capacity for proliferation. Furthermore, the loss of *FTO* also reduces the neuronal and glial differentiation of aNSCs, suggesting the multipotency of aNSCs is impaired in the absence of *Fto*. Together, these results indicate that FTO is not only important for the function of neuronal cells but also critical for the 'stemness' and multipotency of aNSCs.

FTO is known to possess the demethylase activity of m^6A in mRNAs. Both previous works and our present study show that m^6A is not evenly distributed across transcripts, but rather specifically enriched around stop codons, in 3'UTRs, and within long internal exons of RNA (40,41). m^6A modification is enriched in brain and increases during postnatal brain development, and is well conserved between mouse and human (40–42). In *Drosophila*, m^6A is critical for sex determination and controls synaptic growth and neuromuscular junction (42,43). The m^6A modification dynamics mediated by FTO are found to be involved in the dopaminergic signaling pathway and neuronal response to cocaine (16,39). Further, m^6A modification increases in response to behavioral training and promotes cued fear memory retention by affecting the degradation of transcripts (15). Our previous study has shown that FTO could regulate the expression of BDNF through its demethylase activity (23). Our present study also reveals the dynamics of m^6A modification during postnatal neurodevelopment, and m6A-marked mRNAs highly overlap with the genes regulated by FTO as determined by gene expression profiling, including the BDNF signaling pathway. Together, these results suggest FTO plays roles in modulating the activity of aNSCs by regulating m^6A modification of selective transcripts, which could in turn influence their gene expression (38,42–44).

In summary, our current work uncovers an important role of FTO in the regulation of adult neurogenesis. Loss of FTO could diminish the aNSC pool and reduce both proliferation and differentiation of aNSCs, which leads to impaired learning and memory. Our m^6A profiling reveals the dynamics of m^6A modification during postnatal neurodevelopment. By combining m^6A profiling with gene expression analyses, we have identified the key mRNAs modified by m^6A, which could be mediated by FTO. The altered m^6A modification of these transcripts, particularly genes involved in the BDNF pathway, may contribute to the adult neurogenesis deficits associated with the loss of FTO.

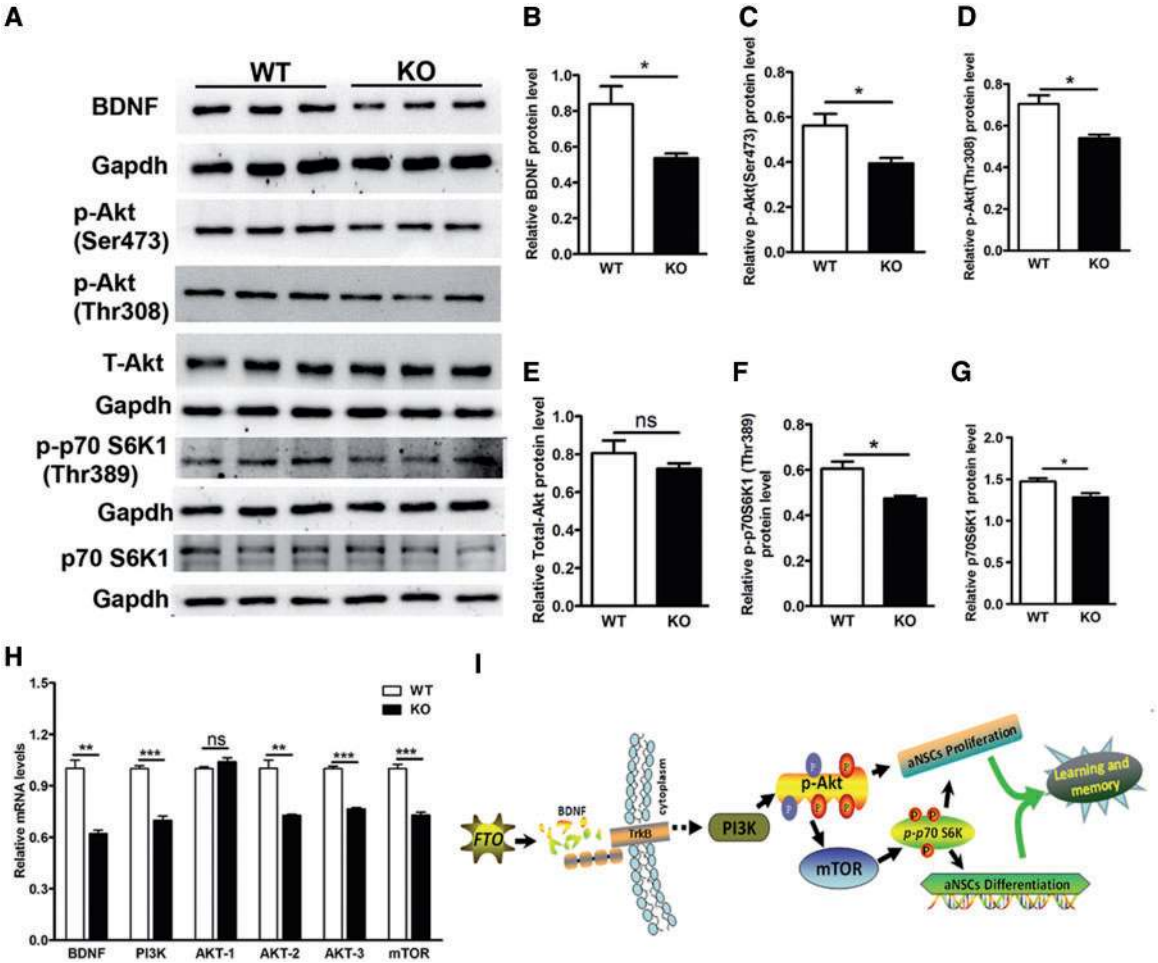

Figure 7. FTO regulates adult neurogenesis through modulation of the BDNF/Akt signaling pathway. (**A**) Representative western blotting images showing the protein levels of BDNF, phospho-Akt, total Akt (T-Akt), phospho-p70S6K1 and total p70S6K1 (p70S6K1). GAPDH was used as a loading control. (**B–G**) Quantification results indicated the protein levels of BDNF (B), phospho-Akt (Ser473) (C), phospho-Akt (Thr308) (D) and phorspho-p70S6K (Thr389) (F) significantly decreased in KO mice compared to WT mice, while the levels of total Akt (E) and p70S6K1 did not change (G). $n = 3$, unpaired *t*-test, $^{*}P < 0.05$. (**H**) BDNF, PI3K, AKT and mTOR mRNA transcripts were detected in the hippocampus of WT and *FTO* KO mice by real-time PCR ($n = 3$). 18s mRNA levels were used as an internal control. Unpaired *t*-test, $^{**}P < 0.01$; $^{***}P < 0.001$. (**I**) Schematic illustration of FTO-mediated regulation of adult neurogenesis.

Materials and Methods

Animals

FTO knockout (KO) mice were generated as described previously (12). Adult (8–12 weeks old) male wild-type (WT) and KO male mice were adopted for the most of study, and female mice were only included for testing the brain and body weight. Mice were housed on a 12 h light/dark schedule and fed *ad libitum*. All experiments were conducted following the protocols approved by The Animal Ethics Committee of Zhejiang University.

BrdU administration and brain section preparation

To evaluate the percentage of cell proliferation and differentiation *in vivo*, adult WT and KO mice were injected with 5'-bromo-2'-deoxyuridine (BrdU) intraperitoneally (50 mg/kg). To assess the proliferation of aNSCs, batches of WT and KO animals were injected with BrdU (i.p.) within 24 h. Mice were sacrificed for study 4 h after the last injection. To assess the differentiation of aNSCs, the other two batches of mice were given BrdU for 3 consecutive days (twice daily at 10 h intervals). Mice were sacrificed at 1 or 4 week(s) after the final BrdU injection.

At the scheduled time point, mice were deeply anesthetized with chloral hydrate (50 mg/kg, i.p.) and transcardially perfused with cold phosphate-buffered saline (PBS), followed by perfusion of 4% PFA. Brains were gently removed and post-fixed in 4% PFA overnight at 4 °C. Twenty-four hours later, the brain samples were transferred into 30% sucrose solution for dehydration at 4 °C. The brain samples were embedded in O.C.T. (Thermo Fisher Scientific) and sectioned in the coronal plane (20 μm) with a cryostat (Leica).

Immunofluorescence staining and cell quantification

For proliferation and differentiation assays, floating brain sections were picked up every 1-in-6 in series, and a total of 8–10 sections were used from each animal. Brain sections were washed with PBS for 30 min, and then were blocked with PBS containing 5% normal goat serum (Vector Laboratories, CA) and 0.1% Triton X-100 for 1 h at room temperature. Sections then were incubated with primary antibodies overnight at 4 °C. For BrdU immunostaining, the sections were pretreated with

1M HCl and incubated at 37 °C for 30 min. The following primary antibodies were used: rabbit anti-FTO (Thermo; PA1-46310), mouse anti-Nestin (BD Pharmingen; 556309), mouse anti-Neuronal Nuclei (NeuN, Millipore; MAB377), rat anti-BrdU (Abcam; ab-6326), rabbit anti-Doublecortin (Cell Signaling Technology; #4604), and rabbit anti-Ki-67 (Millipore; AB9260. On the second day, samples were washed with PBS for 30 min, and then incubated with secondary antibodies for 1 h at room temperature. Fluorophore-conjugated secondary antibody was used: goat anti-mouse Alexa Fluor 568 (Invitrogen; A11031), goat anti-rat Alexa Fluor 568 (Invitrogen; A11077), goat anti-rabbit Alexa Fluor 488 (Invitrogen; A11008), and goat anti-mouse Alexa Fluor 488 (Invitrogen; A11001). DNA was counterstained with the fluorescent nuclear dye 4'6-diamidino-2-phenylindole (DAPI, Sigma-Aldrich, #B2261). After final washes, sections were mounted onto glass slides and cover slipped with mounting medium (Vector Laboratories, CA). All immunostaining experiments were repeated with sections from at least three animals of each genotype.

Immunostained sections were viewed and images were taken with an Olympus confocal microscope (Olympus IX81-FV1000). The numbers of $BrdU^+$, $Ki67^+$, DCX^+ and TUNEL staining positive cells were quantified. The length of main dendrites and the number of DCX+ cells were determined using Image J software.

Nissl staining

Once mounted onto glass slides, the brain sections were successively immersed in 70, 80, 95 and 100% ethanol concentrations to gradually dehydrate for 5 s, respectively. Afterwards, slides were transferred to xylene for 30 s. Subsequently, sections were rehydrated by ethanol from high concentration to low concentration. After washing with ddH_2O, sections were incubated with Nissl staining solution at 37 °C for 30 min. Finally, 70% ethanol was used for decoloration, and 50% glycerinum in PBS was used as mounting medium.

TUNEL staining

To detect apoptotic neurons in the hippocampus and the SVZ of the lateral ventricles, terminal uridine deoxynucleotidyl transferase (dUTP) nick end labeling (TUNEL) staining was performed using a commercial kit (In Situ Cell Death Detection Kit, TMR red; Roche, 12156792910) following the manufacturer's instructions. The brain sections were rinsed 3 times in PBS and covered with proteinase K at 37 °C for 30 min. They were then washed with PBS to terminate enzymatic activity. Finally, slides were incubated with permeabilization solution (0.1% Triton X-100, 0.1% sodium citrate) for 10 min. They were then treated with a TUNEL reaction mixture containing 90% terminal deoxynucleotidyl transferase (TdT) buffer, 5% dUTP-biotin and in 5% TdT in a humid dark box at 3 °C for 1 h. After being rinsed three times in PBS, sections were counterstained with DAPI. In particular, positive control sections were incubated in permeabilization solution with DNase I (3 U/μl) for 10 min at room temperature before reacting with TdT enzyme. However, negative controls were incubated with labeling solution (without terminal transferase) instead of the TUNEL reaction mixture. TUNEL-positive cells in the hippocampus and lateral ventricles were counted in six inconsecutive sections with an Olympus confocal microscope.

Western blot

Hippocampus tissues were ground in ice-cold lysis buffer (150 mM sodium chloride; 1.0% NP-40 or Triton X-100; 0.5% sodium deoxycholate; 0.1% SDS (sodium dodecyl sulphate); 50 mM Tris, pH 8.0) containing 1X protease inhibitor cocktail (Sigma). The homogenates were transferred into a pre-cooled microfuge tube, centrifuged at 4 °C for 20 min at 20 817*g*, and the supernatants were collected. Protein concentrations of the samples were measured by a BioPhotometer (Eppendorf), and 30 μg of proteins of each sample were used for electrophoresis. The following primary antibodies were used: anti-*FTO* (Thermo, PA1-46310), anti-BDNF (Abcam, ab108319), anti-phospho-AKT (Ser473) (Cell Signaling Technology, #4060), anti-phospho-AKT (Thr308) (Cell Signaling Technology, #13038p), anti-AKT (Cell Signaling Technology, 4691p), anti-phospho-p70 S6 Kinase (Thr389) (Cell Signaling Technology, #9234s), anti-p70 S6 kinase (Cell Signaling Technology, #2708) and anti-GAPDH (Ambion, AM4300). The images were visualized and taken using a Molecular Imager Imaging System (Tanon, China). The intensity of images was analyzed with Adobe Photoshop software.

Total RNA isolation, reverse transcription and quantitative real-time PCR

Hippocampus tissues were dissected and homogenized with TRIzol reagent (Ambion). Total RNA was isolated, and the concentration was quantified using a NanoDrop 2000 Spectrophotometer. One microgram of total RNA was used for reverse transcription (RT) (Invitrogen). Standard real-time qPCR was performed using power SYBR Green PCR master Mix (Invitrogen). All real-time PCR reactions were performed in triplicate, and the results were analyzed using the $^{\Delta\Delta}$Ct method.

RNA-seq

Total RNAs were extracted from adult WT and KO hippocampus tissues using TRIzol for RNA-seq. Residual genomic DNA was removed and RNA was purified following standard protocol. All samples used for the cDNA library had an excellent purity as assessed by NanoDrop 2000, and the RNA integrity value (RIN) showed no visible signs of degradation (RIN $\geq$ 9) in an Agilent 2100 Bioanalyzer (Agilent Technologies Inc., Santa Clara, CA, USA). The extracted mRNA was fragmented, reverse transcribed into cDNA, and ligated with proprietary adapters to the 3′ and 5′ termini. Subsequently, paired-end sequencing was performed with the Illumina HiSeq sequencing technology (Illumina, San Diego, USA). Raw sequencing output was filtered, and the retained clean reads were then aligned to the *Mus musculus* reference genome.

m^6A-RIP-seq

Total cellular RNA was purified from fresh mouse hippocampi using the TRIzol Reagent (Invitrogen) according to the manufacturer's instructions. For each biological replicate, the total cellular RNA samples isolated from the hippocampi of 12 wild-type C57BL/6J (B6) mice of the same age were pooled. Polyadenylated RNA was enriched by oligo-dT selection using the PolyATtract mRNA Isolation System (Promega), and then was fragmented into ~100-nt pieces as previously described (45). Fragmented RNA was cleaned and concentrated using the RNA Clean & Concentrator-5 (Zymo Research) with on-column DNase treatment. About 2 μg of RNA fragments were used as the input for

each m6A immunoprecipitation (m^6A-IP). m^6A-IP was performed as previously described (45). Eluted RNA fragments were recovered by adding Pellet Paint Co-Precipitant (EMD Millipore), followed by ethanol precipitation. RNA-seq libraries were generated from recovered RNA fragments of two biological replicates per age group, using the TruSeq LT RNA Library Preparation Kit v2 (Illumina) following the manufacturer's protocol, but skipping the step of mRNA purification and fragmentation. A Qubit dsDNA HS Assay Kit (Invitrogen) and an Agilent 2100 BioAnalyzer with DNA1000 Kit (Agilent) were used to quantify amplified cDNA and to control the quality of the libraries. Illumina HiSeq2000 was used to perform 100-cycle single-read (SR) sequences. Image processing and sequence extraction were done using the standard cloud-based Illumina pipeline in BaseSpace (Illumina).

Bioinformatic analyses of m^6A-IP-seq data

RNA-seq reads were first aligned to the mouse genome (mm9) by Bowtie v2.2.3 (46) using the local, sensitive and non-deterministic mode. m^6A peaks were identified by HOMER findPeaks (47) using the factor mode and additional settings (peak size = 100 nt; fragment length = 100 nt; maximum distance used to stitch peaks together = 50; fold change threshold = 3; local fold change = disabled; size of region to search for control tags = 1x peak size; *P*-value threshold = 0.0001; and false-discovery rate (FDR) threshold = 0.001). High-confidence (HC) peaks found in both biological replicates were annotated by HOMER annotatePeaks.pl (47). The annotation of boundary genes was corrected using a Python script. Differential methylation (DM) in m6A-IP-seq data of WT and *FTO* KO midbrain (GSE47217) (16) was analyzed by R using a Bioconductor package exomePeak (2.8.0) (48) to compare normalized reads count between non-IP (input) and m^6A-IP samples by rescaled hypergeometric test. DM regions are defined as the ones with FDR < 0.05, plus fold enrichment of the peaks on the hypermethylated side being consistently larger than 3. The FPKM (Fragments Per Kilobase of transcript per Million mapped reads) values of gene expression were calculated by Tophat2 (2.1.1) (49) and cuffdiff (2.2.1) (50) using genome build mm9. Genome-wide coverage data were scaled by 1 000 000/total read count and visualized by the Integrative Genomics Viewer (51,52). Gene ontology (GO) analyses were performed by the Database for Annotation, Visualization and Integrated Discovery (DAVID) v6.7 (53).

Morris water maze test

The Morris water maze (MWM) was performed as previously described (54). MWM training was performed in a round, water-filled tub (120 cm in diameter) in an environment rich with extra maze cues. Adult (8-week-old) mice were placed in the water maze with their paws touching the wall from four different starting positions (N, S, E, W) in water consistently maintained at 27 °C. At the end of each day of testing, water was drained, and the tank was cleaned with Quatricide. An invisible escape platform (10 cm in diameter) was located in the same spatial location 1 cm below the water surface independent of a subject's start position on a particular trial. In this way subjects would be able to use extra maze cues to determine the platform's location. Each subject was given 4 trials/day with a 15-min interval for 6 days. The maximum trial length was 60 s, and if subjects did not reach the platform in the allotted time, they were manually guided to it. Upon reaching the platform, subjects were left on it for an additional 5 s to allow for survey of the spatial cues in the environment to guide future navigation. After each trial, subjects were dried and kept in a dry plastic holding cage filled with paper towels to allow them to completely dry off. The holding cage was placed half-on, half-off a heating pad. Animals on the heating pad were not left unattended. Twenty-four hours after the final training trial, a probe trial was performed, during which time the platform was removed and the amount of time swimming in the quadrant that previously contained the escape platform during task acquisition was measured over 60 s. All trials were videotaped and analyzed with MazeScan software (Actimetrics, China). The single time-point data were analyzed by Student's *t*-test, and the serial days' data as dependent values were analyzed by two-way ANOVA.

Eight-arm radial maze test

The apparatus consisted of an octagonal platform (60 mm side length) in the center and eight identical extending arms (300 mm × 60 mm × 150 mm). Arms were made of transparent Plexiglas to allow the animal to see visual cues placed in the room. Doors (25 cm high) were located at the entrance of each arm, with dual sensors to detect the animal when all four paws crossed the door. Each arm was equipped with a head-end detector in the end where chocolate was placed to attract the mice. A video tracking system (Med Associates Inc) was used to observe the movement of the mice. Several salient visual cues (a star, a rectangle, a circle, and a triangle) hung constantly on the white wall in the same positions, and an incandescent light bulb was above the apparatus to prevent shadow within the maze. Animals were fasting 24 h before training, and each animal was weighed before and after fasting to adjust the body weight to 80–85% of normal, free-eating animals. On the first day, they were placed in the full-baited maze in which chocolate particles were scattered in the center and the end of the arms in groups of 4 for 10 min, and animals could explore the maze freely to eat the food rewards with all doors opened. On the second and third days, each mouse was put into the maze alone, with chocolate placed only at the ends of the arms. Mice were placed on the center platform for 10 s and allowed to move freely for 10 min or until all chocolate pellets were consumed. During these days, animals were induced to find and eat food only once in each arm. For the next days, only four arms were baited, and food was placed at the end of the same four arms during this session. Mice were allowed to move freely until all chocolate pellets were consumed or the trial lasted for more than 10 min. A reference memory error was counted when animals visited a non-baited arm with all four paws, and working memory was counted when animals went into an arm that was visited previously with all four paws. The maze was cleaned between each mouse to minimize olfactory intra-maze cues.

Statistical analysis

All data are presented as mean ± S.E.M. and were analyzed with GraphPad Prism software (GraphPad Software, CA). For comparisons between two groups, a two-tailed unpaired Student's *t*-test was used. For multiple group comparisons, a two-way ANOVA followed by Tukey's post hoc test was used. A value of $P < 0.05$ was considered statistically significant.

Accession Number

Sequencing data have been deposited to GEO with accession number GSE94098.

Supplementary Material

Supplementary Material is available at *HMG* online.

Acknowledgements

The authors would like to thank C. Strauss for critical reading of the manuscript and Dr Pumin Zhang for kindly providing *FTO* knockout mice. They thank the Li lab members for technical help.

Conflict of Interest statement. None declared.

Funding

X.L. was supported in part by grants from the National Natural Science Foundation of China (31371309, 31571518) and the National Key Basic Research Program of China (No. 2014CB943001). P.J. was supported in part by grants from the National Institutes of Health (NS051630, NS079625, NS091859, HG008935, and MH102690).

References

1. Gage, F.H. (2000) Mammalian neural stem cells. *Science*, **287**, 1433–1438.
2. Christian, K.M., Song, H. and Ming, G.L. (2014) Functions and dysfunctions of adult hippocampal neurogenesis. *Annu. Rev. Neurosci.*, **37**, 243–262.
3. Deng, W., Aimone, J.B. and Gage, F.H. (2010) New neurons and new memories: how does adult hippocampal neurogenesis affect learning and memory?. *Nat. Rev. Neurosci.*, **11**, 339–350.
4. Hsieh, J. and Zhao, X. (2016) Genetics and epigenetics in adult neurogenesis. *Cold Spring Harb. Perspect. Biol.*, **8**, 336ra61.
5. Alunni, A. and Bally-Cuif, L. (2016) A comparative view of regenerative neurogenesis in vertebrates. *Development*, **143**, 741–753.
6. Li, X. and Jin, P. (2010) Roles of small regulatory RNAs in determining neuronal identity. *Nat. Rev. Neurosci.*, **11**, 329–338.
7. Yao, B., Christian, K.M., He, C., Jin, P., Ming, G.L. and Song, H. (2016) Epigenetic mechanisms in neurogenesis. *Nat. Rev. Neurosci.*, **17**, 537–549.
8. Avgustinova, A. and Benitah, S.A. (2016) Epigenetic control of adult stem cell function. *Nat. Rev. Mol. Cell Biol.*,**17**, 643–658.
9. Church, C., Moir, L., McMurray, F., Girard, C., Banks, G.T., Teboul, L., Wells, S., Bruning, J.C., Nolan, P.M., Ashcroft, F.M. *et al.* (2010) Overexpression of Fto leads to increased food intake and results in obesity. *Nat. Genet.*, **42**, 1086–1092.
10. Fischer, J., Koch, L., Emmerling, C., Vierkotten, J., Peters, T., Bruning, J.C. and Ruther, U. (2009) Inactivation of the Fto gene protects from obesity. *Nature*, **458**, 894–898.
11. Zhao, X., Yang, Y., Sun, B.F., Shi, Y., Yang, X., Xiao, W., Hao, Y.J., Ping, X.L., Chen, Y.S., Wang, W.J. *et al.* (2014) FTO-dependent demethylation of N6-methyladenosine regulates mRNA splicing and is required for adipogenesis. *Cell Res.*, **24**, 1403–1419.
12. Gao, X., Shin, Y.H., Li, M., Wang, F., Tong, Q. and Zhang, P. (2010) The fat mass and obesity associated gene FTO functions in the brain to regulate postnatal growth in mice. *PLoS One*, **5**, e14005.
13. McTaggart, J.S., Lee, S., Iberl, M., Church, C., Cox, R.D. and Ashcroft, F.M. (2011) FTO is expressed in neurones throughout the brain and its expression is unaltered by fasting. *PLoS One*, **6**, e27968.
14. Ho, A.J., Stein, J.L., Hua, X., Lee, S., Hibar, D.P., Leow, A.D., Dinov, I.D., Toga, A.W., Saykin, A.J., Shen, L. *et al.* (2010) A commonly carried allele of the obesity-related FTO gene is associated with reduced brain volume in the healthy elderly. *Proc. Natl. Acad. Sci. U. S. A.*, **107**, 8404–8409.
15. Widagdo, J., Zhao, Q.Y., Kempen, M.J., Tan, M.C., Ratnu, V.S., Wei, W., Leighton, L., Spadaro, P.A., Edson, J., Anggono, V. *et al.* (2016) Experience-dependent accumulation of N6-methyladenosine in the prefrontal cortex is associated with memory processes in mice. *J. Neurosci.*, **36**, 6771–6777.
16. Hess, M.E., Hess, S., Meyer, K.D., Verhagen, L.A., Koch, L., Bronneke, H.S., Dietrich, M.O., Jordan, S.D., Saletore, Y., Elemento, O. *et al.* (2013) The fat mass and obesity associated gene (Fto) regulates activity of the dopaminergic midbrain circuitry. *Nat. Neurosci.*, **16**, 1042–1048.
17. Jia, G., Fu, Y., Zhao, X., Dai, Q., Zheng, G., Yang, Y., Yi, C., Lindahl, T., Pan, T., Yang, Y.G. *et al.* (2011) N6-methyladenosine in nuclear RNA is a major substrate of the obesity-associated FTO. *Nat. Chem. Biol.*, **7**, 885–887.
18. Beemon, K. and Keith, J. (1977) Localization of N6-methyladenosine in the Rous sarcoma virus genome. *J. Mol. Biol.*, **113**, 165–179.
19. Carroll, S.M., Narayan, P. and Rottman, F.M. (1990) N6-methyladenosine residues in an intron-specific region of prolactin pre-mRNA. *Mol. Cell Biol.*, **10**, 4456–4465.
20. Niu, Y., Zhao, X., Wu, Y.S., Li, M.M., Wang, X.J. and Yang, Y.G. (2013) N6-methyl-adenosine (m6A) in RNA: an old modification with a novel epigenetic function. *GenomicsProteomics Bioinformatics*, **11**, 8–17.
21. Jia, G., Fu, Y. and He, C. (2013) Reversible RNA adenosine methylation in biological regulation. *Trends Genet.*, **29**, 108–115.
22. Meyer, K.D., Saletore, Y., Zumbo, P., Elemento, O., Mason, C.E. and Jaffrey, S.R. (2012) Comprehensive analysis of mRNA methylation reveals enrichment in 3' UTRs and near stop codons. *Cell*, **149**, 1635–1646.
23. Lin, L., Hales, C.M., Garber, K. and Jin, P. (2014) Fat mass and obesity-associated (FTO) protein interacts with CaMKII and modulates the activity of CREB signaling pathway. *Hum. Mol. Genet.*, **23**, 3299–3306.
24. Zimmermann, T., Remmers, F., Lutz, B. and Leschik, J. (2016) ESC-derived BDNF-overexpressing neural progenitors differentially promote recovery in Huntington's disease models by enhanced striatal differentiation. *Stem Cell Rep.*, **7**, 693–706.
25. Boschen, K.E., McKeown, S.E., Roth, T.L. and Klintsova, A.Y. (2016) Impact of exercise and a complex environment on hippocampal dendritic morphology, Bdnf gene expression, and DNA methylation in male rat pups neonatally exposed to alcohol. *Dev. Neurobiol.*, doi: 10.1002/dneu.22448. [Epub ahead of print].
26. Kuipers, S.D., Trentani, A., Tiron, A., Mao, X., Kuhl, D. and Bramham, C.R. (2016) BDNF-induced LTP is associated with rapid Arc/Arg3.1-dependent enhancement in adult hippocampal neurogenesis. *Sci. Rep.*, **6**, 21222.
27. Gao, Y., Su, J., Guo, W., Polich, E.D., Magyar, D.P., Xing, Y., Li, H., Smrt, R.D., Chang, Q. and Zhao, X. (2015) Inhibition of

miR-15a promotes BDNF expression and rescues dendritic maturation deficits in MeCP2-deficient neurons. *Stem Cells*, **33**, 1618–1629.
28. Karra, E., O'Daly, O.G., Choudhury, A.I., Yousseif, A., Millership, S., Neary, M.T., Scott, W.R., Chandarana, K., Manning, S., Hess, M.E. *et al.* (2013) A link between FTO, ghrelin, and impaired brain food-cue responsivity. *J. Clin. Invest.*, **123**, 3539–3551.
29. Wiemerslage, L., Nilsson, E.K., Solstrand Dahlberg, L., Ence-Eriksson, F., Castillo, S., Larsen, A.L., Bylund, S.B., Hogenkamp, P.S., Olivo, G., Bandstein, M. *et al.* (2016) An obesity-associated risk allele within the FTO gene affects human brain activity for areas important for emotion, impulse control and reward in response to food images. *Eur. J. Neurosci.*, **43**, 1173–1180.
30. Melka, M.G., Gillis, J., Bernard, M., Abrahamowicz, M., Chakravarty, M.M., Leonard, G.T., Perron, M., Richer, L., Veillette, S., Banaschewski, T. *et al.* (2013) FTO, obesity and the adolescent brain. *Hum. Mol. Genet.*, **22**, 1050–1058.
31. Ma, D.K., Marchetto, M.C., Guo, J.U., Ming, G.L., Gage, F.H. and Song, H. (2010) Epigenetic choreographers of neurogenesis in the adult mammalian brain. *Nat. Neurosci.*, **13**, 1338–1344.
32. Avgustinova, A. and Benitah, S.A. (2016) Epigenetic control of adult stem cell function. *Nat. Rev. Mol. Cell Biol.*, **17**, 643–658.
33. Fu, Y., Dominissini, D., Rechavi, G. and He, C. (2014) Gene expression regulation mediated through reversible m(6)A RNA methylation. *Nat. Rev. Genet.*, **15**, 293–306.
34. Meyer, K.D. and Jaffrey, S.R. (2014) The dynamic epitranscriptome: N6-methyladenosine and gene expression control. *Nat. Rev. Mol. Cell Biol.*, **15**, 313–326.
35. Wang, Y., Li, Y., Toth, J.I., Petroski, M.D., Zhang, Z. and Zhao, J.C. (2014) N6-methyladenosine modification destabilizes developmental regulators in embryonic stem cells. *Nat. Cell Biol.*, **16**, 191–198.
36. Geula, S., Moshitch-Moshkovitz, S., Dominissini, D., Mansour, A.A., Kol, N., Salmon-Divon, M., Hershkovitz, V., Peer, E., Mor, N., Manor, Y.S. *et al.* (2015) Stem cells. m6A mRNA methylation facilitates resolution of naive pluripotency toward differentiation. *Science*, **347**, 1002–1006.
37. Batista, P.J., Molinie, B., Wang, J., Qu, K., Zhang, J., Li, L., Bouley, D.M., Lujan, E., Haddad, B., Daneshvar, K. *et al.* (2014) m(6)A RNA modification controls cell fate transition in mammalian embryonic stem cells. *Cell Stem Cell*, **15**, 707–719.
38. Nainar, S., Marshall, P.R., Tyler, C.R., Spitale, R.C. and Bredy, T.W. (2016) Evolving insights into RNA modifications and their functional diversity in the brain. *Nat. Neurosci.*, **19**, 1292–1298.
39. Sevgi, M., Rigoux, L., Kuhn, A.B., Mauer, J., Schilbach, L., Hess, M.E., Gruendler, T.O., Ullsperger, M., Stephan, K.E., Bruning, J.C. *et al.* (2015) An obesity-predisposing variant of the FTO gene regulates D2R-dependent reward learning. *J. Neurosci.*, **35**, 12584–12592.
40. Meyer, K.D., Patil, D.P., Zhou, J., Zinoviev, A., Skabkin, M.A., Elemento, O., Pestova, T.V., Qian, S.B. and Jaffrey, S.R. (2015) 5' UTR m(6)A promotes cap-independent translation. *Cell*, **163**, 999–1010.
41. Dominissini, D., Moshitch-Moshkovitz, S., Schwartz, S., Salmon-Divon, M., Ungar, L., Osenberg, S., Cesarkas, K., Jacob-Hirsch, J., Amariglio, N., Kupiec, M. *et al.* (2012) Topology of the human and mouse m6A RNA methylomes revealed by m6A-seq. *Nature*, **485**, 201–206.
42. Lence, T., Akhtar, J., Bayer, M., Schmid, K., Spindler, L., Ho, C.H., Kreim, N., Andrade-Navarro, M.A., Poeck, B., Helm, M. *et al.* (2016) m6A modulates neuronal functions and sex determination in Drosophila. *Nature*, **540**, 242–247.
43. Haussmann, I.U., Bodi, Z., Sanchez-Moran, E., Mongan, N.P., Archer, N., Fray, R.G. and Soller, M. (2016) m6A potentiates Sxl alternative pre-mRNA splicing for robust Drosophila sex determination. *Nature*, 540, 301–304.
44. Yue, Y., Liu, J. and He, C. (2015) RNA N6-methyladenosine methylation in post-transcriptional gene expression regulation. *Genes. Dev.*, **29**, 1343–1355.
45. Dominissini, D., Moshitch-Moshkovitz, S., Salmon-Divon, M., Amariglio, N. and Rechavi, G. (2013) Transcriptome-wide mapping of N(6)-methyladenosine by m(6)A-seq based on immunocapturing and massively parallel sequencing. *Nat. Protoc.*, **8**, 176–189.
46. Langmead, B. and Salzberg, S.L. (2012) Fast gapped-read alignment with Bowtie 2. *Nat. Methods*, **9**, 357–359.
47. Heinz, S., Benner, C., Spann, N., Bertolino, E., Lin, Y.C., Laslo, P., Cheng, J.X., Murre, C., Singh, H. and Glass, C.K. (2010) Simple combinations of lineage-determining transcription factors prime cis-regulatory elements required for macrophage and B cell identities. *Mol. Cell*, **38**, 576–589.
48. Meng, J., Cui, X., Rao, M.K., Chen, Y. and Huang, Y. (2013) Exome-based analysis for RNA epigenome sequencing data. *Bioinformatics*, **29**, 1565–1567.
49. Kim, D., Pertea, G., Trapnell, C., Pimentel, H., Kelley, R. and Salzberg, S.L. (2013) TopHat2: accurate alignment of transcriptomes in the presence of insertions, deletions and gene fusions. *Genome Biol.*, **14**, R36.
50. Trapnell, C., Hendrickson, D.G., Sauvageau, M., Goff, L., Rinn, J.L. and Pachter, L. (2013) Differential analysis of gene regulation at transcript resolution with RNA-seq. *Nat. Biotechnol.*, **31**, 46–53.
51. Robinson, J.T., Thorvaldsdottir, H., Winckler, W., Guttman, M., Lander, E.S., Getz, G. and Mesirov, J.P. (2011) *Nat. Biotechnol.*, **29**, 24–26.
52. Thorvaldsdottir, H., Robinson, J.T. and Mesirov, J.P. (2013) Integrative Genomics Viewer (IGV): high-performance genomics data visualization and exploration. *Brief. Bioinform.*, **14**, 178–192.
53. Huang da, W., Sherman, B.T. and Lempicki, R.A. (2009) Systematic and integrative analysis of large gene lists using DAVID bioinformatics resources. *Nat. Protoc.*, **4**, 44–57.
54. Hong, Y., Chan, C.B., Kwon, I.S., Li, X., Song, M., Lee, H.P., Liu, X., Sompol, P., Jin, P., Lee, H.G. *et al.* (2012) SRPK2 phosphorylates tau and mediates the cognitive defects in Alzheimer's disease. *J. Neurosci.*, **32**, 17262–17272.